An Efficient Two-Phase L^1-TV Method for Restoring Blurred Images with Impulse Noise

Raymond H. Chan, Yiqiu Dong, and Michael Hintermüller

Abstract

A two-phase image restoration method based on total variation regularization combined with an L^1-data-fitting term for impulse noise removal and deblurring is proposed. In the first phase, suitable noise detectors are used for identifying image pixels contaminated by noise. Then, in the second phase, based on the information on the location of noise-free pixels, images are deblurred and denoised simultaneously. For efficiency reasons, in the second phase a superlinearly convergent algorithm based on Fenchel-duality and inexact semismooth Newton techniques is utilized for solving the associated variational problem. Numerical results prove the new method to be a significantly advance over several state-of-the-art techniques with respect to restoration capability and computational efficiency.

Index Terms

Fenchel duality, image deblurring, impulse noise, L^1 data fitting, noise detector, total variation regularization, semismooth Newton method.

I. Introduction

During their acquisition and transmission images are often blurred and corrupted by noise. It is one of the fundamental tasks of image processing to restore the (original) image from a degraded version. To be

Raymond H. Chan is with Department of Mathematics, The Chinese University of Hong Kong, Shatin, Hong Kong (email: rchan@math.cuhk.edu.hk). Research is supported by HKRGC under grant no. CUHK 400508.

Yiqiu Dong and Michael Hintermüller are with START-Project "Interfaces and Free Boundaries" and SFB "Mathematical Optimization and Applications in Biomedical Science", Institute of Mathematics and Scientific Computing, University of Graz, Heinrichstrasse 36, A-8010 Graz, Austria (email: yiqiu.dong, michael.hintermueller@uni-graz.at). Research is supported by the Austrian Science Fund FWF under SFB F32 "Mathematical Optimization and Applications in Biomedical Science" and the Austrian Ministry of Science and Research under START-grant Y305 "Interfaces and Free Boundaries".

Michael Hintermüller is also with Department of Mathematics, Humboldt-University of Berlin, Unter den Linden 6, 10099 Berlin, Germany (email: hint@math.hu-berlin.de).

specific, suppose an image $u \in \mathbb{R}^{mn}$ is blurred by a known linear operator (matrix) $K \in \mathbb{R}^{mn \times mn}$, where m-by-n, with $m, n \in \mathbb{N}$, is the image size. Due to transmission errors, malfunctioning pixel elements in camera sensors, faulty memory locations, etc., the blurred image is also assumed to be corrupted by impulse noise [1]. Consequently, the degraded image $z \in \mathbb{R}^{mn}$ can be written as

$$z = N_r(\tilde{z}) \quad \text{with} \quad \tilde{z} = Ku,$$

where N_r represents the corruption by impulse noise with a corruption rate $r \in [0, 1]$. Based on the gray-level values of the noisy pixels, there are mainly two types of impulse noise:

- *Salt-and-pepper noise:*

$$z_k = \begin{cases} \tilde{z}_k, & \text{with probability } 1 - r, \\ n_{\max}, & \text{with probability } \frac{r}{2}, \\ n_{\min}, & \text{with probability } \frac{r}{2}, \end{cases}$$

  where $n_{\max}$ and $n_{\min}$ are the maximum and minimum of the gray-level range.

- *Random-valued impulse noise:*

$$z_k = \begin{cases} \tilde{z}_k, & \text{with probability } 1 - r, \\ n_k, & \text{with probability } r, \end{cases}$$

  where n_k comes from a uniformly distributed random variable with values in $[n_{\min}, n_{\max}]$.

An important characteristic of impulse noise is that only a part of the pixels is corrupted by noise and the rest is noise-free. Since the noise may produce arbitrary values in $[n_{\min}, n_{\max}]$, random-valued impulse noise is more difficult to remove than salt-and-pepper noise. Over the years, a variety of techniques have been proposed to remove impulse noise. Here we refer to [2]–[7] for salt-and-pepper noise and to [8]–[12] for random-valued impulse noise removal, respectively, as well as to the many references in these papers. In the corresponding methods, typically only the denoising case is considered, i.e., $K = I$, with I the identity operator.

The deblurring of images, however, poses some additional challenges when compared to the denoising case. In fact, image deblurring is an ill-posed problem due to either the potential non-uniqueness of the solution or the numerical instability respectively induced by K. To alleviate these problems and the difficulties due to the noise in the data, some a-priori preferences are usually added in the form of a regularization term such as Tikhonov [13], total variation [14], or wavelet coefficient [15] regularization. In the case of degradation due to impulse noise, regularization combined with L^1 data fitting was proposed for restoration; see [16]–[20]. Typically, the pertinent methods are implemented uniformly across the image without considering whether a pixel is noise-free or not. In order to benefit from the fact that some part

of the pixels is noise-free, in [21] a two-phase method relying on noise detectors was proposed. In the first or noise detecting phase, it uses either the adaptive median (AM) filter [2] or the adaptive center-weighted median (ACWM) filter [8] to identify pixels which are likely to contain noise. In the second phase, based on the identified noise-free pixels, the image is deblurred and denoised simultaneously using the Mumford-Shah function. Numerical results show that this two-phase method can give excellent restoration results when compared with the several state-of-the-art techniques which are implemented uniformly across the whole image. But since the algorithm of [21] relies on an alternating fixed point iteration, it is not efficient with respect to its convergence rate. Furthermore, there are three crucial parameters which need to be adjusted based on information generated during the restoration. Together with the fixed point-type iteration, the necessary parameter adjustment based on computational outcomes results in a rather time-consuming method requiring intensive user interaction.

Recently, in [20] a locally superlinearly convergent algorithm for solving the L^1-TV problem (see (1) below) was introduced. Its very efficient implementation can compete successfully with several recent methods proposed, e.g., in [16], [17], [19]. In the present paper, we combine the method of [20] with the noise detectors of [2], [8], [12] to obtain an efficient two-phase method. By efficiency we refer here to a local (at least) superlinear convergence of the associated numerical method in the second phase and the significantly reduced effort in parameter adjustment. In fact, with total variation as the choice for the regularization term, the optimization problem in the second phase is solved by a superlinearly convergent algorithm based on Fenchel-duality and inexact semismooth Newton techniques. The new two-phase method outperforms the old one in [21] with respect to both image restoration capability and computational efficiency. Indeed, compared to our method in our numerical tests, the technique of [21] consumes 20 to 49 times more CPU-time. Furthermore, for our method the effect of the parameters in the optimization problem in the second phase is well understood. In the end, only the total variation regularization parameter needs to be determined once at the beginning of the iteration in contrast to the selection of three parameters based on the currently restored image in [21]. In addition, since the capability of the two-phase method hinges on the accuracy of the noise detector in the first phase, among others we also utilize the newest statistic,which is called rank-ordered logarithmic difference (ROLD, for short) [12], as a noise detector when restoring images with a high corruption by random-valued impulse noise. Our experiments show that we obtain an 1.5 dB improvement in peak signal-to-noise ratio (PSNR) for corruption rates as high as 60% when compared with the technique in [21].

The outline of this paper is as follows. In Section II, we extend the method in [20] by incorporating information on noise-free pixels. Section III describes our two-phase method in detail. Section IV provides

numerical results to demonstrate the performance of the new algorithm. Finally, conclusions are drawn in Section V.

II. Image Restoration by Primal-Dual Algorithm

Recently, in [20] an efficient method was proposed to restore images corrputed by impulse noise by solving the following minimization problem, which we call the L^1-TV problem:

$$\min_{u\in\mathbb{R}^{mn}} \|Ku - z\|_1 + \alpha\|u\|_{TV}, \tag{1}$$

where $\|v\|_1 = \sum_{k\in\mathcal{A}} |v_k|$, $\mathcal{A}$ is the so-called candidate (index) set of all pixels in the image, $\alpha > 0$ is the regularization parameter which controls the trade-off between the L^1-data-fitting term and the total variation regularization, which is defined by

$$\|v\|_{TV} := \sum_{k\in\mathcal{A}} |[\nabla v]_k|_2 = \sum_{k\in\mathcal{A}} \sqrt{|(\nabla_x v)_k|^2 + |(\nabla_y v)_k|^2}$$

with the discrete gradient operator $\nabla \in \mathbb{R}^{2mn\times mn}$, with

$$\nabla = \begin{bmatrix} \nabla_x \\ \nabla_y \end{bmatrix} \quad \text{and} \quad [\nabla v]_k = \begin{bmatrix} (\nabla_x v)_k \\ (\nabla_y v)_k \end{bmatrix},$$

where $\nabla_x, \nabla_y \in \mathbb{R}^{mn\times mn}$ and

$$(\nabla_x v)_k = \begin{cases} v_{i+1,j} - v_{i,j}, & \text{if } i < m, \\ 0, & \text{if } i = m, \end{cases} \qquad (\nabla_y v)_k = \begin{cases} v_{i,j+1} - v_{i,j}, & \text{if } j < n, \\ 0, & \text{if } j = n, \end{cases}$$

and $k = (i-1)\cdot n + j$, $i \in \{1, 2, \cdots, m\}$, $j \in \{1, 2, \cdots, n\}$. For the efficient solution of (1), Fenchel-duality [22] and inexact semismooth Newton techniques [23] are utilized. In view of the characteristics of impulse noise, i.e., only a part of the pixels is corrupted, we equip the Newton solver with an appropriate noise detector. For this purpose, we assume that the noise candidate set obtained by a noise detector is $\mathcal{N}$ and the noise-free candidate set is $\mathcal{U} = \mathcal{A} \setminus \mathcal{N}$.

Noise-free pixels in the image correspond to intensity values according to the blurring model $z = Ku$. The presence of impulse noise, however, destroys this relation. Hence, in what follows we ignore noisy pixels in the data-fitting term of (1) by removing $\mathcal{N}$ from $\mathcal{A}$ in the first term of the objective function in (1). This results in the following minimization problem:

$$\min_{u\in\mathbb{R}^{mn}} \sum_{k\in\mathcal{U}} |(Ku)_k - z_k| + \alpha \sum_{k\in\mathcal{A}} |[\nabla u]_k|_2. \tag{$\mathcal{P}$}$$

Our aim is to apply the primal-dual method of [20] to solve $(\mathcal{P})$. Hence, in the first step we compute the Fenchel-dual of $(\mathcal{P})$. For this purpose, let

$$\Psi(u) := \sum_{k\in\mathcal{U}} |(Ku)_k - z_k|\,,$$
$$\Phi(\vec{p}) := \alpha \sum_{k\in\mathcal{A}} |[\vec{p}]_k|_2, \qquad \vec{p} := \nabla u \in \mathbb{R}^{2mn}.$$

The Fenchel-conjugate of Ψ is defined by $\Psi^*(w) = \sup\{u^\top w - \Psi(u) | u \in \mathbb{R}^{mn}\}$ [22], and analogously for Φ. After some calculations, we get

$$\Psi^*(w) = \sum_{k\in\mathcal{U}} z_k \cdot \left((KK^\top)^{-1}Kw\right)_k + I_{\{v:|((KK^\top)^{-1}Kv)_k|\le 1, k\in\mathcal{U}\}}(w),$$
$$\Phi^*(\vec{q}) = I_{\{\vec{w}:|[\vec{w}]_k|_2\le\alpha, k\in\mathcal{A}\}}(\vec{q}),$$

where $w \in \mathbb{R}^{mn}$ and $\vec{q} \in \mathbb{R}^{2mn}$. Here, $K^\top$ is the transpose of K, and $I_S(\cdot)$ denotes the indicator function of the set S. Furthermore, we assume that $KK^\top$ rather than K is invertible. This assumption allows us to consider a more general problem class where the blurring operator K need not be a square matrix. An example for the latter is a situation where the image z is not only blurred and corrupted by impulse noise, but also loses some information after blurring; see [20]. In such a situation, also the dimension of the data vector z needs to be adjusted correspondingly. We proceed on the basis of such a general setting; otherwise one assumes that K is invertible and replaces $(KK^\top)^{-1}K$ by $K^{-\top}$ in what follows.

The following relation between the primal (left hand side) and the dual problem (right hand side) holds true:

$$\inf_{u\in\mathbb{R}^{mn}} \{\Psi(u) + \Phi(\Lambda u)\} = \sup_{q\in\mathbb{R}^{2mn}} \{-\Psi^*(\Lambda^\top q) - \Phi^*(-q)\}, \tag{2}$$

where $\Lambda \in \mathbb{R}^{2mn\times mn}$, and $\Lambda^\top$ is the transpose of Λ. Due to the structure of Ψ^* and Φ^*, the dual problem can be written as follows:

$$\min_{\vec{q}\in\mathbb{R}^{2mn}} \sum_{k\in\mathcal{U}} z_k \cdot \left((KK^\top)^{-1}K\nabla^\top\vec{q}\right)_k, \tag{$\mathcal{P}^*$}$$
$$\text{subject to (s. t.) } |((KK^\top)^{-1}K\nabla^\top\vec{q})_k| \le 1, \quad \forall k \in \mathcal{U},$$
$$|[\vec{q}]_k|_2 \le \alpha, \qquad\qquad \forall k \in \mathcal{A}.$$

Note that due to the presence of the divergence operator $\mathrm{div} = -\nabla^\top$, which has a non-trivial kernel, in the objective function of $(\mathcal{P}^*)$, the solution to $(\mathcal{P}^*)$ need not be unique. In order to achieve uniqueness, which is beneficial from a numerical stability point of view, we add a dual regularization term. The

resulting problem is given by

$$\min_{\vec{q}\in\mathbb{R}^{2mn}} \sum_{k\in\mathcal{U}} z_k \cdot \left((KK^\top)^{-1}K\nabla^\top\vec{q}\right)_k + \frac{\gamma}{2\alpha}\sum_{k\in\mathcal{A}} |[\vec{q}]_k|_2^2, \qquad (\mathcal{P}_\gamma{}^*)$$
$$\text{s. t. } |((KK^\top)^{-1}K\nabla^\top\vec{q})_k| \le 1, \quad \forall k \in \mathcal{U},$$
$$|[\vec{q}]_k|_2 \le \alpha, \qquad \forall k \in \mathcal{A},$$

where $\gamma > 0$ denotes the corresponding dual regularization parameter. From an algorithmic point of view, due to its smooth objective and rather simple contraints $(\mathcal{P}_\gamma{}^*)$ is more amenable to fast solvers than $(\mathcal{P})$. The latter usually rely on the first order optimality conditions for the associated minimization problem. In our case, the first order conditions of $(\mathcal{P}_\gamma{}^*)$ are given by

$$-\mathrm{div}\bar{\vec{p}} = K^\top\chi_{\mathcal{U}}\sigma(K\bar{u}-z) \quad \text{with} \quad \sigma(K\bar{u}-z) \in \partial\|K\bar{u}-z\|_1, \tag{3a}$$
$$-[\bar{\vec{p}}]_k = \alpha\frac{[\nabla\bar{u}]_k}{\max\{\gamma, |[\nabla\bar{u}]_k|_2\}}, \tag{3b}$$

for $k = 1, \dots, nm$, where the characteristic function of the set $\mathcal{U}$ is written as a diagonal matrix $\chi_{\mathcal{U}} \in \mathbb{R}^{mn\times mn}$ defined by

$$(\chi_{\mathcal{U}})_{k,k} = \begin{cases} 1, & \text{if } k \in \mathcal{U}, \\ 0, & \text{if } k \in \mathcal{N}. \end{cases}$$

Moreover, ∂ denotes the subdifferential of convex analysis [22] and, for $v \in \mathbb{R}^t$, with $t \in \mathbb{N}$, $\sigma(v) \in \partial\|v\|_1 \subset \mathbb{R}^t$ satisfies

$$(\sigma(v))_i \in \begin{cases} \{1\} & \text{if } v_i > 0, \\ \{-1\} & \text{if } v_i < 0, \\ [-1,1] & \text{if } v_i = 0, \end{cases}$$

for $i = 1, \dots, r$. We observe that given $\vec{p}$, (3) does not allow to recover u, in general. For this reason we replace $(\mathcal{P}_\gamma{}^*)$ by $(\mathcal{P}^*_{\lambda,\gamma})$:

$$\min_{\vec{q}\in\mathbb{R}^{2mn}} \sum_{k\in\mathcal{U}} z_k \cdot \left((KK^\top)^{-1}K\nabla^\top\vec{q}\right)_k + \frac{\lambda}{2}\sum_{k\in\mathcal{U}} \left((KK^\top)^{-1}K\nabla^\top\vec{q}\right)_k^2 + \frac{\gamma}{2\alpha}\sum_{k\in\mathcal{A}} |[\vec{q}]_k|_2^2, \qquad (\mathcal{P}^*_{\lambda,\gamma})$$
$$\text{s.t. } |((KK^\top)^{-1}K\nabla^\top\vec{q})_k| \le 1, \quad \forall k \in \mathcal{U},$$
$$|[\vec{q}]_k|_2 \le \alpha, \qquad \forall k \in \mathcal{A},$$

where $\lambda > 0$ is given.

In order to understand the effect of replacing $(\mathcal{P}^*)$ by $(\mathcal{P}^*_{\lambda,\gamma})$ on the primal problem $(\mathcal{P})$, we dualize $(\mathcal{P}^*_{\lambda,\gamma})$. In view of the general relation (2) in convex analysis and $\mathrm{div} = -\nabla^\top$, we now define

$$\Psi^*(\mathrm{div}\vec{q}) := \sum_{k\in\mathcal{U}} z_k \cdot \left((KK^\top)^{-1}K\nabla^\top\vec{q}\right)_k + \frac{\lambda}{2}\sum_{k\in\mathcal{U}} \left((KK^\top)^{-1}K\nabla^\top\vec{q}\right)_k^2$$

$$+ I_{\{v:|((KK^\top)^{-1}Kv)_k|\leq 1, k\in\mathcal{U}\}}(\nabla^\top \vec{q}),$$

$$\Phi^*(\vec{q}) := \frac{\gamma}{2\alpha}\sum_{k\in\mathcal{A}} |[\vec{q}]_k|_2^2 + I_{\{\vec{w}:|[\vec{w}]_k|_2\leq\alpha, k\in\mathcal{A}\}}(\vec{q}).$$

Upon calculating the associated Fenchel conjugates, we find that the Fenchel dual of $(\mathcal{P}^*_{\lambda,\gamma})$ is given by

$$\min_{u\in\mathbb{R}^{mn}} \sum_{k\in\mathcal{A}} (\Psi_\lambda(u))_k + (\Phi_\gamma(\nabla u))_k\,, \tag{$\mathcal{P}_{\lambda,\gamma}$}$$

where

$$(\Psi_\lambda(u))_k = \begin{cases} \frac{1}{2\lambda}\left((Ku)_k - z_k\right)^2, & \text{if } |(Ku)_k - z_k| < \lambda \text{ and } k\in\mathcal{U}, \\ |(Ku)_k - z_k| - \frac{\lambda}{2}, & \text{if } |(Ku)_k - z_k| \geq \lambda \text{ and } k\in\mathcal{U}, \\ 0, & \text{if } k\in\mathcal{N}, \end{cases}$$

and

$$(\Phi_\gamma(\nabla u))_k = \begin{cases} \frac{\alpha}{2\gamma}|[\nabla u]_k|_2^2\,, & \text{if } |[\nabla u]_k|_2 < \gamma, \\ \alpha\left[|[\nabla u]_k|_2 - \frac{\gamma}{2}\right], & \text{if } |[\nabla u]_k|_2 \geq \gamma. \end{cases}$$

We observe that the uniqueness of the solution of the regularized dual $(\mathcal{P}^*_{\lambda,\gamma})$ is due to Φ_γ. Without the second regularization, a reconstruction of the primal solution $\bar{u}$ from a dual solution $\bar{\vec{p}}$ would not be possible. This explains the purpose of Ψ_λ.

By first order optimality and $\nabla^\top = -\mathrm{div}$, the solutions $\bar{u}$ and $\bar{\vec{p}}$ satisfy

$$-\mathrm{div}\bar{\vec{p}} = K^\top \chi_{\mathcal{U}} \sigma_\lambda(K\bar{u} - z), \tag{4a}$$

$$\bar{[\vec{p}]}_k = \frac{-\alpha}{\max\{\gamma, |[\nabla\bar{u}]_k|_2\}}[\nabla\bar{u}]_k, \tag{4b}$$

for $k = 1,\ldots,nm$, where we have $\sigma_\lambda(K\bar{u} - z)\in\mathbb{R}^{mn}$ with

$$\sigma_\lambda(K\bar{u} - z)_k = \frac{(K\bar{u} - z)_k}{\max\{\lambda, |(K\bar{u} - z)_k|\}}.$$

Note that the terms $\max\{\lambda, |(K\bar{u} - z)_k|\}$ and $\max\{\gamma, |[\nabla\bar{u}]_k|_2\}$ are always positive. In order to make the system (4a)–(4b) more tractable from a numerical point of view, we introduce

$$\bar{v} := \sigma_\lambda(K\bar{u} - z) \quad \text{and} \quad \bar{\vec{s}} := -\bar{\vec{p}}.$$

Then the sytem (4a)–(4b) is equivalent to

$$-D(m_\lambda)\bar{v} + K\bar{u} - z = 0, \tag{5a}$$

$$\mathrm{div}\bar{\vec{s}} - K^\top\chi_{\mathcal{U}}\bar{v} = 0, \tag{5b}$$

$$D(m_\gamma)\bar{\vec{s}} - \alpha\nabla\bar{u} = 0. \tag{5c}$$

Here, $D(v)\in\mathbb{R}^{t\times t}$ is a diagonal matrix with the vector $v\in\mathbb{R}^t$ as its main diagonal, $m_\lambda\in\mathbb{R}^{mn}$ with $(m_\lambda)_k = \max\{\lambda, |(K\bar{u} - z)_k|\}$, $m_\gamma\in\mathbb{R}^{2mn}$ with $(m_\gamma)_k = (m_\gamma)_{mn+k} = \max\{\gamma, |[\nabla\bar{u}]_k|_2\}$, and we

use $|w| = (|w_1|, \ldots, |w_{mn}|)^\top$ for $w \in \mathbb{R}^{mn}$. Moreover, $|\nabla v|_2 = (|[\nabla v]_1|_2, \ldots, |[\nabla v]_{mn}|_2)^\top \in \mathbb{R}^{mn}$ for $v \in \mathbb{R}^{mn}$.

Note that the system (5) is non-smooth due to the presence of the max-operators. However, it can be shown that (5) is semismooth [24]. This allows us to utilize the semismooth Newton technique of [25] for its numerical solution. For this purpose, we write (5) compactly as

$$F(\bar{\omega}) = 0,$$

with $\bar{\omega} = (\bar{u}, \bar{v}, \bar{\vec{s}})$. Given a current iterate ω^l approximating $\bar{\omega}$, the corresponding semismooth Newton update δ_ω^l is defined as the solution of

$$G(\omega^l)\delta_\omega^l = -F(\omega^l), \tag{6}$$

with $\delta_{\omega,l} = \omega_{l+1} - \omega^l$, provided such a solution exists. In (6) we have $G(\omega^l) \in \partial F(\omega^l)$ with $\partial F(\omega^l)$ denoting the generalized derivative of F according to [24]. We note that the subdifferential of convex analysis (i.e. Clarke's subdifferential [26]) is a special realization of the generalized derivative defined in [24]. A particular choice of $G(\omega^l)$ is given by

$$G(\omega^l) = \begin{bmatrix} A^l & -D(m_\lambda^l) & 0 \\ 0 & -K^\top \chi_{\mathcal{U}} & -\nabla^\top \\ B^l & 0 & D(m_\gamma^l) \end{bmatrix},$$

where

$$A^l = \left[I_{mn} - D(v^l)\chi_{\mathcal{A}_\lambda^l} D(\operatorname{sign}(Ku^l - z))\right] K := \Lambda^l K,$$
$$B^l = \left[-\alpha I_{2mn} + D(s^l)D(g^l)N(\nabla u^l)\right] \nabla := -C^l \nabla,$$

and $g^l \in \mathbb{R}^{2mn}$ with

$$g_k^l = g_{mn+k}^l = \frac{1}{|[\nabla u^l]_k|_2} \quad \text{for } k \in \mathcal{A}_\gamma^l \quad \text{and} \quad g_k^l = g_{mn+k}^l = 0 \quad \text{else.}$$

Here, $I_t \in \mathbb{R}^{t\times t}$ is the identity matrix, $\mathcal{A}_\lambda^l = \{k : |(Ku^l)_k - z_k| > \lambda\}$, and $\mathcal{A}_\gamma^l = \{k : |[\nabla u^l]_k|_2 > \gamma\}$. In addition, for $w = (w_1^\top, w_2^\top)^\top \in \mathbb{R}^{2t}$, with $w_i \in \mathbb{R}^t$ for $i \in \{1, 2\}$, we use

$$N(w) = \begin{bmatrix} D(w_1) & D(w_2) \\ D(w_1) & D(w_2) \end{bmatrix} \in \mathbb{R}^{2t\times 2t}.$$

The structure of $G(\omega^l)$ allows us to condense the Newton system (6) into a single equation

$$H^l \delta_u = f^l, \tag{7}$$

with

$$H^l = K^\top \chi_{\mathcal{U}} D(m_\lambda^l)^{-1} \Lambda^l K + \nabla^\top D(m_\gamma^l)^{-1} C^l \nabla,$$
$$f^l = -K^\top \chi_{\mathcal{U}} D(m_\lambda^l)^{-1} (Ku^l - z) - \alpha \nabla^\top D(m_\gamma^l)^{-1} \nabla u^l.$$

The system matrix in (7) may lack symmetry and/or positive definiteness along the iterations; however, at a solution, the matrix is symmetric positive semi-definite. In order to avoid problems due to these potential deficiencies during the iteration, we utilize the modifications as introduced in [20], whenever these are necessary. This results in a modified system matrix $H_+^l + \mu^l I_{mn}$ (instead of H^l in (7)), where μ^l is a small positive value approaching zero as l increases.

III. Our Two-Phase Method

In this section we provide an overall description of our two-phase method, discuss the use of noise detectors, and we specify the parameter choice.

In the first phase, we use a noise detector to distinguish pixels which are likely to be corrupted by impulse noise, i.e., we determine the noise candidate set $\mathcal{N}$. For salt-and-pepper noise, we choose the adaptive median (AM) filter [2], which, by varying the window size, can identify almost all noisy pixels even for corruption rates as high as 90%. For random-valued impulse noise, as in [21] we utilize the adaptive center-weighted median (ACWM) filter [8] for comparison. This filter is able to distinguish most of the noisy pixels from the noise-free ones with a small false-hit rate for low corruption rates. When the corruption rate reaches 60%, we observe that the capabilities of the two-phase method are mainly limited by the accuracy of the noise detector ACWM in the first phase. In order to remedy this drawback, we replace the ACWM filter by the rank-ordered logarithmic difference (ROLD statistic) [12], which was proposed recently in particular for detecting random-valued impulse noise with a high corruption rate.

After the noise detection step, in the second phase we use the available information on noise-free pixels, i.e., $k \in \mathcal{U}$, to simultaneously deblur and denoise the given image by solving the minimization problem $(\mathcal{P}_{\lambda,\gamma})$. As described in the previous section, based on first order optimality, the numerical solution is achieved by inexact semismooth Newton techniques. Note that in the objective function of $(\mathcal{P}_{\lambda,\gamma})$, both Ψ_λ and Φ_γ are in fact Huber-type functions [27]. Hence, our approach results in a nonlinear hybrid L^1-L^2 measure, which smoothes only in a region near zero. In Ψ_λ and Φ_γ, λ and γ are the Huber thresholds, which control the balance between the respective L^1 and L^2 terms. The smaller these two parameters are, the more challenging the solution of the minimization problem becomes. This behavior can be attributed to the fact that uniform convexity and, hence, uniqueness of the solution as well as the reconstructability

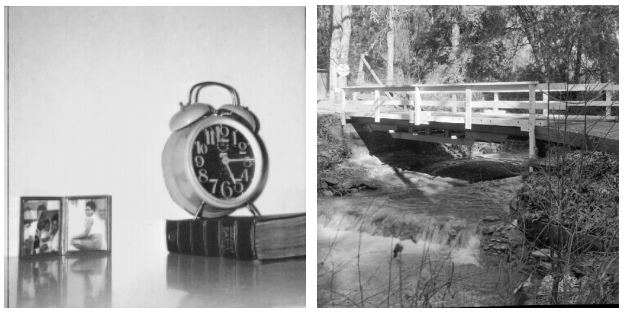

(a) (b)

Fig. 1. Original images. (a) “Clock”, (b) “Bridge”.

of a primal solution from a dual one get lost for $\lambda = \gamma = 0$. Here, based on our numerical experiments, we fix the values $\lambda = 0.0005$ and $\gamma = 0.01$. The remaining parameter α is the regularization parameter, which controls the trade-off between a good fit of z and a smoothness requirement due to the total variation regularization. This suggests that small α is used for low corruption rates in order to preserve details with little smoothing, and large α is used for high corruption rates in order to remove noise considerably. The precise choice of α for the respective restoration run is provided in the captions of the subsequent figures.

IV. Numerical Results

In this section, we compare the image restoration ability and CPU-time consumption of our method only with the two-phase method in [21] (the CCN method for short), which was shown to outperform state-of-the-art methods which are implemented uniformly across the whole image for deblurring and denoising. For illustrations, the results for the 256-by-256 gray level image “Clock” and the 512-by-512 gray level image “Bridge” are presented. The original images, which we show in Figure 1, can be found in [28]. The quality of the restoration results is compared quantitatively by using the peak signal-to-noise ration (PSNR) [1] which is defined as

$$\text{PSNR} = 10 \log_{10} \frac{n_{\max}^2}{\frac{1}{mn} \sum_{k=1}^{mn} (\tilde{u}_k - u_k)^2} \quad (dB),$$

where $\tilde{u}_k$ and u_k denote the pixel values of the restored image and the original image, respectively; and $n_{\max}$ is the maximum of the gray-level range, which we set to 1 in our tests.

In Tables I and II, we list the best PSNR values for both methods for the two images with different corruption rates and blurring operators. For the CCN method, based on the suggestions in [21], we fix η

TABLE I

COMPARISON OF RESTORATION RESULTS IN PSNR (DB) FOR IMAGES BLURRED BY DIFFERENT BLURRING OPERATORS AND CORRUPTED BY SALT-AND-PEPPER NOISE.

Image	r	Gaussian		Out-of-focus		Motion	
		CCN	Our	CCN	Our	CCN	Our
Clock	30%	32.09	38.52	32.53	38.97	32.42	37.04
	50%	31.20	35.88	31.21	35.09	30.57	32.93
	70%	29.56	32.44	29.14	30.74	28.25	29.18
Bridge	30%	28.07	31.31	30.05	31.90	30.69	31.78
	50%	27.46	29.37	28.30	28.89	28.47	28.86
	70%	26.41	27.09	26.48	26.62	26.18	26.32

to 0.0001 and adjusted the remaining three parameters α, β, ϵ one after the other through numerical tests until they become stable. For our method, we only need to determinate the regularization parameter α as described at the end of Section III. In our experiments, we consider three different blurring operators, which are Gaussian blur with a window size of 7×7 and a standard deviation of 5, out-of-focus blur with radius 3, and motion blur with length 9 and angle 1.

For detecting salt-and-pepper noise, we use the AM filter [2] with a maximum window size of 19. From Table I it is clear that for all images, blurring operators and corruption rates, our method gives better PSNR values when compared to the CCN method. Especially when the corruption rate is less than 50% or the images are subject to Gaussian blur, our method performs much better. To compare the results visually, we display the restored images in Figures 2 and 3. Figure 2 shows an enlarged part of the results of the CCN method and our method for restoring the Gaussian blurred image "Clock" with salt-and-pepper noise. We find that ringing artifacts are noticeable in the background in the results obtained by the CCN method; compare Figures 2 (c) and (d) in the first row. Since we utilize total variation regularization in our method, those spurious rings are absent from our results, but at the same time there might be some undesirable stair-casing effects; see the housing of the clock in Figure 2 (d) in the second row. This phenomenon is typical for total variation regularization. Furthermore, we observe that our method works well for preserving details, compare the numbers in the clock in Figure 2. In addition, in Figure 3 we enlarge a part of the restored image "Bridge" for different blurring operators

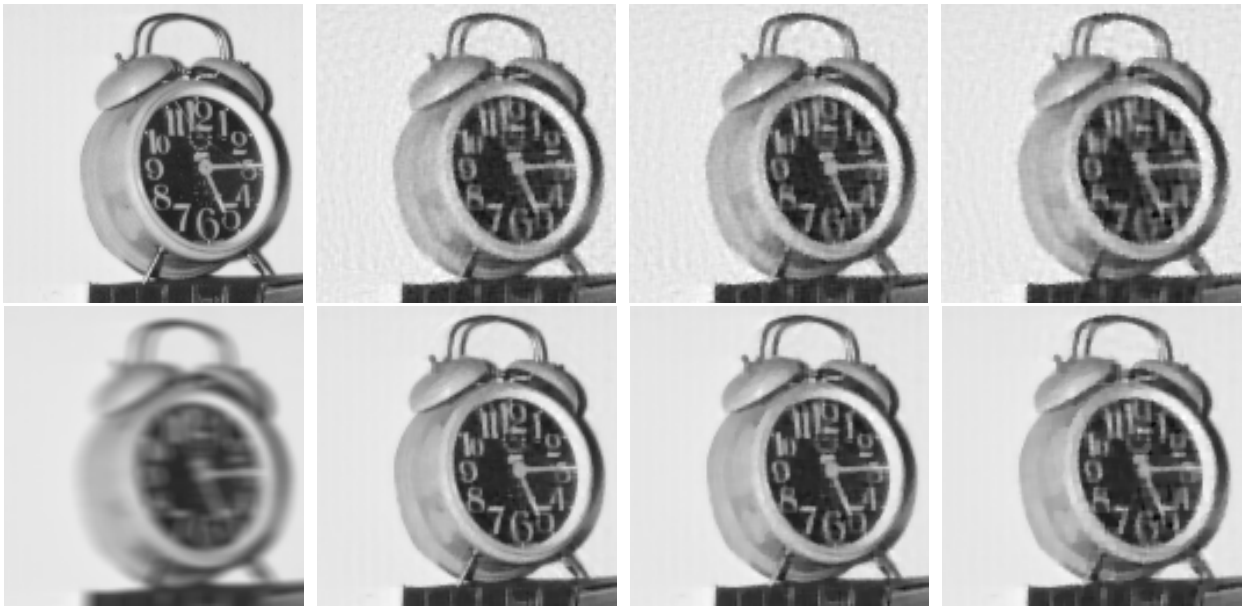

(a) (b) (c) (d)

Fig. 2. Results of the CCN method (the first row) and our method (the second row) when restoring the Gaussian blurred image "Clock" with salt-and-pepper noise: (a) original image (the first row) and blurred image (the second row), (b) $r = 30\%$, (c) $r = 50\%$, (d) $r = 70\%$. The parameter α in our method is 0.004 for (b), 0.006 for (c), 0.007 for (d).

and 50% salt-and-pepper noise in order to compare the CCN method with our method. Apparently, in all cases our method outperforms the CCN method concerning the preservation of details such as the edges of the bridge.

In Table II, we show the PSNR values when restoring the blurred images with random-valued impulse noise. In the first phase, we use the ACWM filter [8] as the noise detector. It is clear that for all images, blurring operators, and corruption rates, our method gives better PSNR values than the CCN method. Figure 4 shows the enlarged portion of the corresponding results for restoring images degraded by out-of-focus blur and 20% or 40% random-valued impulse noise. We find that our method preserves more details and no ringing artifacts occur near the edges; see, e.g., the background in Figure 4 (b) and the the edges of the bridge in Figure 4 (d). Furthermore, Figure 5 shows restoration results for the image "Bridge" which is subject to different types of blurring and 60% random-valued impulse noise. When the corruption rate is as high as 60%, the restoration results of the CCN method [21] and of our method with the ACWM filter suffer from noticeable noise patches. The main cause is the inadequacy of the ACWM filter for detecting noisy pixels under high corruption rates. As a remedy, we use the ROLD

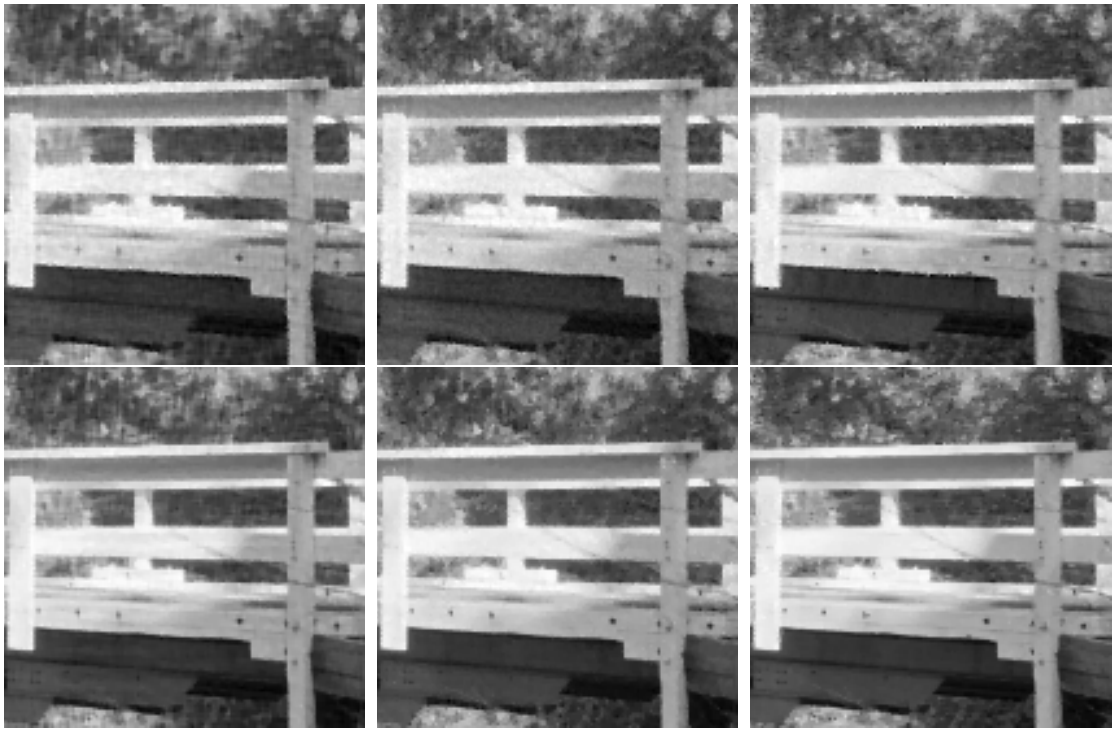

(a) (b) (c)

Fig. 3. Results of the CCN method (the first row) and our method (the second row) when restoring the blurred image "Bridge" with different blurring operators and 50% salt-and-pepper noise: (a) Gaussian blur, (b) out-of-focus blur, (c) motion blur. The parameter α in our method is 0.003 for (a), 0.011 for (b) and 0.015 for (c).

statistic [12] as the noise detector. The latter was especially designed for high corruption rates. It is, however, less effective for moderate and small corruption rates. In Table II we provide the PSNR values of the restoration results in italic font, and display the resulting images in the third row of Figure 5. We observe that compared with the two methods discussed earlier, the visual quality is obviously improved, and the PSNR values are more than 1 dB higher.

For the comparison of the computational efficiency, in Tables III and IV, CPU-time ratios are presented with our method as the base reference. For a fair comparison, every experiment is repeated 10 times, and the associated average is shown here. Since in both of the two-phase methods, the second phase consumes most of the total CPU-time and is based on the same noise detector, respectively, we only list the CPU-time ratios associated with the second phase. Upon comparing the results in Tables III and IV, we find that our method clearly outperforms the CCN method. Especially when restoring the blurred image with 60% random-valued impulse noise, the CCN method takes 40 times more CPU-time than our

TABLE II

COMPARISON OF RESTORATION RESULTS IN PSNR (DB) FOR IMAGES BLURRED BY DIFFERENT BLURRING OPERATORS AND CORRUPTED BY RANDOM-VALUED IMPULSE NOISE.

Image	r	Gaussian		Out-of-focus		Motion	
		CCN	Our	CCN	Our	CCN	Our
Clock	20%	32.17	38.23	32.63	39.09	31.53	35.59
	40%	30.82	34.93	29.87	33.28	27.39	29.65
	60%	22.26	25.98	21.89	25.72	20.68	24.36
			29.33		*27.67*		*25.97*
Bridge	20%	28.22	31.49	30.11	32.06	29.48	30.97
	40%	27.45	28.84	27.82	28.38	26.14	26.95
	60%	24.45	24.73	21.47	24.53	22.28	23.49
			25.99		*25.68*		*24.54*

TABLE III

THE CPU-TIME RATIOS FOR THE IMAGES BLURRED WITH OUT-OF-FOCUS BLURRING OPERATOR AND CORRUPTED BY SALT-AND-PEPPER NOISE.

Method	Clock			Bridge		
	30%	50%	70%	30%	50%	70%
$\frac{\text{CCN}}{\text{Our}}$	20.5	20.2	21.2	22.1	25.7	22.7

method. Furthermore, our method requires the adjustment of only one parameter, which follows well-known principles in inverse problems, rather than the selection of three parameters by various numerical tests as in the CCN method. In conclusion, our method turns out to be more efficient than the CCN technique, which was shown in [21] to outperform several state-of-the-art methods.

V. CONCLUSIONS

In this paper, we propose a new efficient two-phase method for restoring images corrupted by some blurring operator and impulse noise. Our approach uses total variation regularization with L^1 data fitting (L^1TV) and combines it with suitable noise detectors. In order to enhance the overall solution method, the

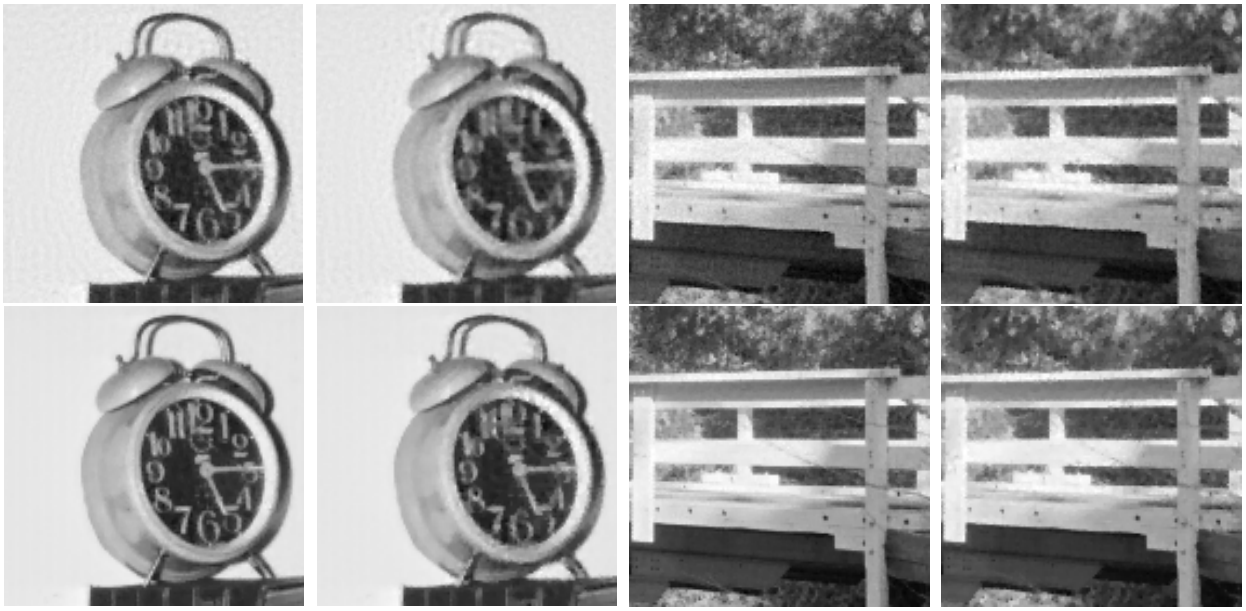

(a) (b) (c) (d)

Fig. 4. Results of the CCN method (the first row) and our method (the second row) when restoring the out-of-focus blurred images with 20% and 40% random-valued impulse noise: (a) $r = 20\%$, (b) $r = 40\%$, (c) $r = 20\%$, (d) $r = 40\%$. The parameter α in our method is 0.021 for (a), 0.032 for (b), 0.015 for (c) and 0.025 for (d).

TABLE IV

THE CPU-TIME RATIOS FOR THE IMAGES BLURRED WITH OUT-OF-FOCUS BLURRING OPERATOR AND CORRUPTED BY RANDOM-VALUED IMPULSE NOISE.

Method	Clock			Bridge		
	20%	40%	60%	20%	40%	60%
$\frac{\text{CCN}}{\text{Our}}$	26.0	28.0	49.8	29.7	35.6	40.5

L^1TV-problem is solved by a superlinearly convergent algorithm based on Fenchel-duality and inexact semismooth Newton techniques. Numerical results show that our method outperforms the very competitive two-phase method of [21], both visually and quantitatively. Furthermore, the CPU-time consumed by our method is significantly smaller than the one consumed by the method of [21].

Finally we mention that we observe test runs, where both methods, the CCN method and our new technique, sometimes yield PSNR-values below 30dB, with the latter considered as a benchmark. We point out that the main limitation here could be the noise detector. In fact, in Table II, for instance, we provide

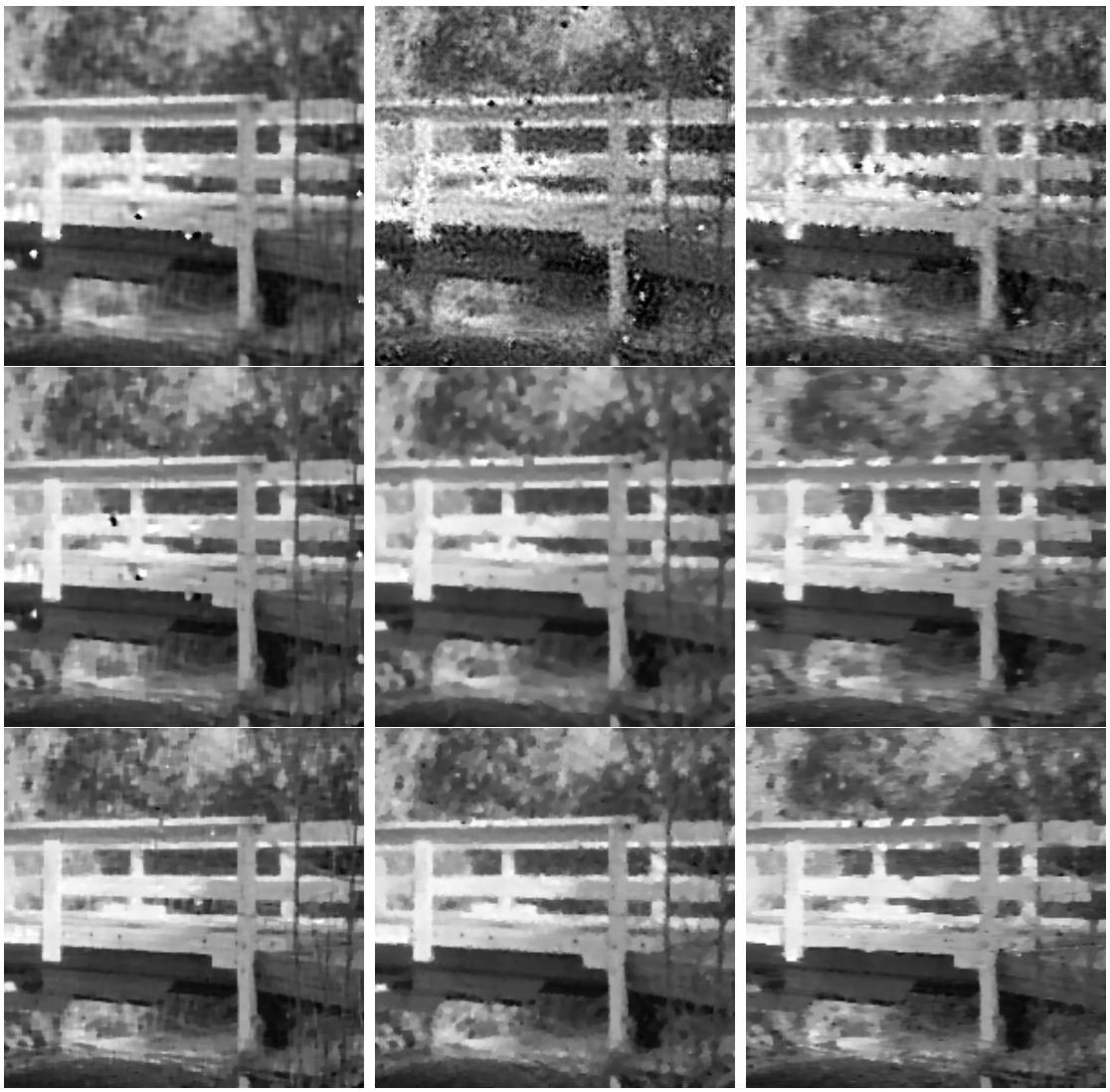

(a) (b) (c)

Fig. 5. Results of the CCN method (the first row), our method with the ACWM filter as noise detector (the second row) and our method with ROLD statistic as noise detector when restoring the blurred image "Bridge" with 60% random-valued impulse noise: (a) Gaussian blur, (b) out-of-focus blur, (c) motion blur.

results for the ACWM filter and the ROLD statistic, respectively, when detecting noisy pixels. In high noise cases we find that ROLD yields a significantly higher dB-value when compared to ACWM. This indicates that our primal-dual algorithm does not limit the overall performance. Further, the investigation of noise detectors which exhibit robustness when detecting corrupted pixels for a broad range of noise levels and types still leaves room for improvement in future research.

ACKNOWLEDGMENT

The authors would like to thank Dr. Jianfeng Cai (University of California, Los Angeles) for providing the code of [21].

REFERENCES

[1] A. Bovik, *Handbook of Image and Video Processing*. Academic Press, 2000.

[2] H. Hwang and R. Haddad, "Adaptive median filters: new algorithms and results," *IEEE Transactions on Image Processing*, vol. 4, pp. 499–502, 1995.

[3] S. Zhang and M. Karim, "A new impulse detector for switching median filters," *IEEE Signal Processing Letters*, vol. 9, pp. 360–363, 2002.

[4] I. Aizenberg, C. Butakoff, and D. Paliy, "Impulsive noise removal using threshold Boolean filtering based on the impulse detecting functions," *IEEE Signal Processing Letters*, vol. 12, pp. 63–66, 2005.

[5] M. Nikolova, "A variational approach to remove outliers and impulse noise," *Journal of Mathematical Imaging and Vision*, vol. 20, pp. 99–120, 2004.

[6] R. Chan, C. Ho, and M. Nikolova, "Salt-and-pepper noise removal by median-type noise detectors and detail-preserving regularization," *IEEE Transactions on Image Processing*, vol. 14, no. 10, pp. 1479–1485, 2005.

[7] R. H. Chan, C.-W. Ho, C.-Y. Leung, and M. Nikolova, "Minimization of detail-preserving regularization functional by Newton's method with continuation," in *ICIP*, 2005, pp. 125–128.

[8] T. Chen and H. Wu, "Adaptive impulse detection using center-weighted median filters," *IEEE Signal Processing Letters*, vol. 8, pp. 1–3, 2001.

[9] R. Chan, Hu, C., and M. Nikolova, "An iterative procedure for removing random-valued impulse noise," *IEEE Signal Processing Letters*, vol. 11, pp. 921–924, 2004.

[10] R. Garnett, T. Huegerich, C. Chui, and W.-J. He, "A universal noise removal algorithm with an impulse detector," *IEEE Transactions on Image Processing*, vol. 14, pp. 1747–1754, 2005.

[11] Y. Dong and S. Xu, "A new directional weighted median filter for removal of random-valued impulse noise," *IEEE Signal Processing Letters*, pp. 193–196, 2007.

[12] Y. Dong, R. H. Chan, and S. Xu, "A detection statistic for random-valued impulse noise," *IEEE Transactions on Image Processing*, vol. 16, pp. 1112–1120, 2007.

[13] A. Tikhonov and V. Arsenin, *Solutions of Ill-Posed Problems*. Winston and Sons, Washington D.C, 1977.

[14] L. Rudin, S. Osher, and E. Fatemi, "Nonlinear total variation based noise removal algorithms," *Physica D*, vol. 60, pp. 259–268, 1992.

[15] J. Bect, L. Blanc-Féraud, G. Aubert, and A. Chambolle, "A l^1-Unified variational framework for image restoration," in *Proc. ECCV'2004*, vol. LNCS, no. 3024. Springer, 2004, pp. 1–13.

[16] L. Bar, N. Sochen, and N. Kiryati, "Image deblurring in the presence of salt-and-pepper noise," in *Proceeding of 5th International Conference on Scale Space and PDE methods in Computer Vision*, vol. LNCS, no. 3439, 2005, pp. 107–118.

[17] ——, "Image deblurring in the presence of impulsive noise," *International Journal of Computer Vision*, vol. 70, pp. 279–298, 2006.

[18] ——, "Deblurring of color images corrupted by salt-and-pepper noise," *IEEE Transactions on Image Processing*, vol. 16, pp. 1101–1111, 2007.

[19] J. Yang, Y. Zhang, and W. Yin, "An efficient TVL1 algorithm for deblurring multichannel images corrupted by impulsive noise," Submitted. URL: http://www.caam.rice.edu/wy1/paperfiles/Rice_CAAM_TR08-12.PDF.

[20] Y. Dong, M. Hintermüller, and M. Neri, "A primal-dual method for L^1 TV image denoising," To appear in SIAM Journal on Imaging Sciences. URL: http://www.uni-graz.at/imawww/ifb/IFB_Report27_HiDoNe09.pdf.

[21] J. Cai, R. Chan, and M. Nikolova, "Two-phase approach for deblurring images corrupted by impulse plus gaussian noise," *Inverse Problems and Imaging*, vol. 2, pp. 187–204, 2008.

[22] I. Ekeland and R. Témam, *Convex Analysis and Variational Problems*. Classics Appl. Math. 28, SIAM, 1999.

[23] M. Hintermüller and G. Stadler, "An infeasible primal-dual algorithm for total bounded variation-based inf-convolution-type image restoration," *SIAM Journal on Scientific Computing*, vol. 28, no. 1, pp. 1–23, 2006.

[24] M. Hintermüller, K. Ito, and K. Kunisch, "The primal-dual active set strategy as a semismooth newton method," *SIAM J. Optim.*, vol. 13, pp. 865–888, 2002.

[25] M. Hintermüller and K. Kunisch, "Total bounded variation regularization as bilaterally constrained optimization problem," *SIAM J. Appl. Math.*, vol. 64, pp. 1311–1333, 2004.

[26] F. M. Clarke, *Optimization and Nonsmooth Analysis*. Wiley Interscience, New York, 1983.

[27] P. J. Huber, "Robust regression: Asymptotics, conjectures, and monte carlo," *Annals of Statistics*, vol. 1, pp. 799–821, 1973.

[28] "USC-SIPI image database," in *http://sipi.usc.edu/services/database/Database.html*. University of Southern California.